Inclusion of Frequency Stability Constraints in Unit Commitment Using Separable Programming

C.J. Ferrandon-Cervantes[a,*], Behzad Kazemtabrizi[a] and Matthias C. M. Troffaes[b]

[a]Durham University, Department of Engineering, Lower Mountjoy, South Road, Durham DH1 3LE
[b]Durham University, Department of Mathematical Sciences, Lower Mountjoy, Stockton Rd, Durham DH1 3LE

ARTICLE INFO

Keywords:
UC
low inertia
linear programming
optimisation
frequency stability

ABSTRACT

In this paper we address the problem of frequency stability in the unit commitment (UC) optimisation process. We include a set of appropriately defined frequency stability constraints in the UC problem formulation for operational planning scenarios in advance of real-time operation. Consequently, we cover the system against the loss of the largest infeed under the $N-1$ security criterion.The main contribution of our work consists of using the method of separable programming to incorporate a linearised Frequency Nadir constraint into the UC problem. In our work, the UC problem is formulated as a mixed-integer linear program (MILP). This renders a fast convergence in the solution for a system such as the the three area IEEE RTS-96 system. Meanwhile, we have included the possibility of synthetic inertia provision from the wind farms, which helps to increase the available inertia in the system before a generation outage. The simulations are run using an extended version of MATPOWER tailored for solving UC problems (MOST) which is run in MATLAB.

1. Introduction

Power Systems have been evolving at a rapid pace in recent years due to the ever increasing levels of renewable generation integration. Consequently, Transmission System Operators (TSOs) are facing a new set of challenges to maintain balance between generation and demand because of the inherent variability of Renewable Energy Resources (RES).This is the case both in terms of distributed generation at the distribution voltage levels, and large-scale offshore wind farms at the transmission voltage levels, which is the scale on which we focus. Indeed, in our work, we are specifically looking at the energy injection from wind farms in the UK [1, 2].

Specifically, we recognize that the large-scale integration of renewable resources, which are often converter-interfaced and thus do not automatically add inertia, coupled with their inherent variability as well as the displacement of conventional resources to maintain with the existing environmental targets will inevitably lead to a reduction in system total inertia which would introduce additional challenges in terms of maintaining frequency stability [3, 4].

The rotational inertia is indeed the first line of defence by the grid following a disturbance (contingency) and it is normally provided by conventional fossil fueled generation which are directly coupled to the grid. Large rotating machines that are synchronised to the grid add the required kinetic energy that damps the effect of a sudden loss of generation, avoiding large frequency excursions in the system[5, 6]. Even though the TSO schedules units to meet a minimum level of inertia, this value on its own is not necessarily enough to safeguard against a frequency excursion, especially in low inertia systems. In the case of the UK, the power system is now more prone than ever to larger frequency excursions in the event of large disturbances due to a sustained reduction of inertia[7]. An even higher level of reduction of inertia is expected for the next 10 years[8], decreasing by 60% lower than that of the current value and exposing the system to greater risk of frequency events.

An example of a recent severe frequency event in the UK was on 9th August, 2019[9]. On this day, the contingency (i.e. the disturbance event) was a N-2 event, caused by the simultaneous outage of two power plants (a wind farm and a combined-cycle power plant, besides an amount of distributed generation in later stages of the event). Consequently, the system did not have the energy to provide sufficient primary frequency response (PFR) to recover the frequency

*CJ Ferrandon-Cervantes is sponsored by Consejo Nacional de Ciencia y Tecnología - Secretaría de Energía (CONACYT-SENER), México
carlos.j.ferrandon-cervantes@durham.ac.uk (C.J. Ferrandon-Cervantes); behzad.kazemtabrizi@durham.ac.uk (B. Kazemtabrizi); matthias.troffaes@durham.ac.uk (M.C.M. Troffaes)
ORCID(s): 0000-0002-4022-4856 (C.J. Ferrandon-Cervantes); 0000-0003-0916-4063 (B. Kazemtabrizi); 0000-0002-1294-600X (M.C.M. Troffaes)

to its safe operational region in a timely manner. PFR is part of a suite of frequency response service provisions by the UK TSO, National Grid ESO. According to National Grid's official definition, PFR is a "response provided within 10 seconds of an event, which can be sustained for a further 20 seconds"[10]. To set a minimum value of inertia and PFR is part of the frequency stability studies required by the System Operator Guideline (SOGL) European Network Code[11].

From an operational planning perspective, it is therefore crucial that TSOs have at their disposal the necessary resources to respond effectively to such large frequency excursions even in low inertia systems. To this end, our aim in this paper is to incorporate the frequency stability constraints within the unit commitment (UC) problem for operational planning purposes.

In this paper, we adopt an $N-1$ security criterion. Generally speaking, this criterion means that at minimum the system must withstand any disturbance (i.e. contingency) caused by the outage of any one single component (e.g. transmission line and/or generator). In our work, we are specifically looking at power imbalances produced by the outage of the largest generator or interconnector. From the TSO perspective, this yields a minimum number of units to be committed in order to withstand a possible frequency excursion due to the loss of the largest infeed. The transient responses from the controls in the wind turbines are not in the scope of this paper.

The Unit Commitment (UC) problem is a mathematical tool with which network operators, namely TSO, determine, over a set planning timescale, an optimum set of generating units that are to be committed to maintain network operational security. When bearing the security of the system in mind, the problem becomes a Security-Constrained Unit Commitment (SCUC). The UC problem, at its core, contains the set of constraints pertaining to the network operational requirements (i.e. nodal power balance constraints, transmission thermal limit constraints, etc.) as well as generating units limits (i.e. maximum capacity, ramp limits, inter-temporal constraints, minimum up and down times, etc.). However, additional constraints such as frequency stability constraints, may be added to the core UC problem if need be [12, 13]. For instance, authors in [14] propose to include the primary and tertiary reserves in the UC problem, which is defined as a multi-period optimisation problem over a 24-hours planning period.

The UC problem formulation may include a stochastic formulation to tackle the inherent uncertainty in renewable resource (e.g. wind) and demand forecasts. For example, in the work of [15], a UC stochastic formulation is used to take into account multiple scenarios of demand and wind realisations. The wind input is modelled as an auto regressive process (AR). The time window of analysis is performed for a whole year of UC optimisation. Transmission network constraints are not considered. The authors in [16] include frequency stability constraints in the UC optimisation by extracting a priori the bounds of the variables that have an influence in the constraints. Although this method runs faster than a piece-wise linearisation of the nonlinear constraints of frequency stability, it is affected by the size of the system. This approach is tested on a 20 synchronous generators system.

More recently, scholars working to overcome the challenges of low-rotational inertia have proposed different approaches to tackle the frequency stability constraints into the unit commitment [17, 18]. In [17] authors use two methods to achieve this: overestimating planes, and binary expansion with the big-M method, whereas in [18] the authors introduce the frequency constraints as mixed integer second order cone program (MISOCP), based on the fact that binary variables and the big-M method is used as well in this approach, when certain conditional statements are met in the proposed formulation. Both of these works are implemented within a stochastic framework and include frequency services with different time responses.

In [19] the virtual inertial response from wind farms are specifically modelled from their mechanical power generated, and the whole problem is solved as a stochastic chance-constrained frequency constrained unit commitment problem. Furthermore, in the work of [20], authors introduce the concept of frequency security margin. This expression is non linear, thus it is linearised via a piecewise linearisation method and using a deterministic unit commitment approach.

Authors in [21] incorporate scenarios with de-loaded modes of wind turbines variable speed, providing PFR and frequency response as well. The way they tackle the non linearity of the Frequency Nadir is by adding binary and continuous variables to the problem. This is all formulated as a stochastic mixed integer linear problem, and solved via Generalised Bender Decomposition (GBD). The work is based on a six-bus system. What differentiates this latest literature from the work presented in this paper is the approach to the nadir non linearity. Whereas the above authors linearise it through the methods mentioned earlier, in our work we approach the nadir linearisation via separable programming.

Indeed, we solve the deterministic UC problem as a mixed integer linear program. We incorporate three sets of frequency stability constraints namely, the Rate of Change of Frequency (RoCoF), the Frequency Nadir and the Quasi

Steady-State Minimum Frequency Recovery. For the three constraints we follow the frequency deviation limits set in the UK grid code by the UK TSO, National Grid ESO [22] to select an acceptable value of RoCoF. Inclusion of the three frequency stability constraints, ensures that within a set planning timescale, the optimum unit commitment schedule not only adheres to the network's operational boundaries but also meets the inertia and PFR requirements to withstand the frequency disturbances due to the loss of the largest in-feed. We use separable programming techniques as a way to linearly approximate the Frequency Nadir constraint, which is nonlinear. Separable programming is a technique for approximating a nonlinear term by a linear term, by translating it into a larger linear program that involves additional binary variables. To apply this technique, the function in question must be in separated terms. This is the case of the Frequency Nadir, which we will elaborate later. This addition of frequency stability constraints makes the UC problem a SCUC one.

To respond to these frequency excursions, in our work we added the possibility of including so-called "synthetic inertia" (SI), or virtual inertia emulation. This response takes advantage of the stored kinetic energy in the rotating blades of the wind turbine. Since wind turbines rotate at a non-synchronous speed, their coupling with the grid frequency is normally provided through a power electronic converter interface, and with the proper control settings, they can provide almost instantaneous power response, as long as the wind turbines have the room to deliver this power to the grid [23]. We assume in this work that the wind turbines are able to deliver this response. We note that time-domain frequency and transient stability analysis is beyond the scope of this research as our focus is on operations planning ahead of real-time operation in form of the solution of a multi-period SCUC problem.

For the test system we use the updated IEEE Reliability Test System [24] using the three areas of the original system, and we run the simulations in a Matlab environment, using a modified version of MOST (Matpower Optimal Scheduling Tool) [25, 26]. The optimisation process is solved via the Gurobi solver.

The paper is organised as follows. In section 2 we describe the UC modelling including frequency stability constraints. In section section 3 we cover the simulation and results obtained. Finally, in section section 5 we draw the conclusions and discuss future work.

2. The UC optimisation process

In the first layer of operational planning power systems we run into the problem of allocating units in order to meet the demand at a certain time point. This is the UC process [27]. Based on the available resources of each unit and the cost of running them, the goal is to minimise the cost of synchronising and desynchronising generators to the grid and meet the demand. This is usually a problem that is run at least a day ahead. The time point has to be coherent with the rate of change of power output of each unit. This is usually performed on hourly or half hourly basis. The UC problem is typically formulated as a mixed integer linear program [28, 29] (MILP), and this is due to the binary decisions that occur to synchronise or disconnecting the units. Other types of problems, such as Network-constrained Unit Commitment, are solved via mixed-integer nonlinear programming [30].

In the next subsection we define the mathematical modelling of the UC applied in this paper.

2.1. UC objective function

The aim is to optimise the objective function in eq. (1) where:

$$\min_{\Phi} \sum_{t\in\mathcal{T}} \sum_{g\in\mathcal{G}} \left(S_g(u_g^t - u_g^{t-1}) + F_g(P_g^t) + C_g^0 u_g^t + C_g^+ R_g^t + \delta_g(P_g^t - P_g^{t-1}) \right) \tag{1}$$

where $\Phi := (P_g^t, R_g^t, u_g^t, \theta_\upsilon^t)_{g\in\mathcal{G}, t\in\mathcal{T}, \upsilon\in\mathcal{M}}$ and where P_g^0 and u_g^0 are known.

- $t \in \mathcal{T} := \{1, \dots, T\}$, where $\mathcal{T}$ is the set containing all timesteps in the planning horizon, and T is the final time point,
- $g \in \mathcal{G} := \{1, \dots, G\}$, where $\mathcal{G}$ is the set containing all synchronous generators, and G is the number of generators,
- u_g^t is the unit status (up or down) of unit g at time t, where $u_g^t \in \{0, 1\}$,
- $S_g(u_g^t - u_g^{t-1}) := C_g^{SU+} \max(u_g^t - u_g^{t-1}, 0) + C_g^{SD-} \max(u_g^{t-1} - u_g^t, 0)$ is the start-up and shutdown cost function which has a unit-dependent costs C_g^{SU+}, C_g^{SD-} per event,

- $F_g(P_g^t)$ is the fuel cost function. In our modelling we use a piecewise linear form where $F_g(P) := \max_{i=1}^{n_g} a_{gi}P + b_{gi}$, with parameters a_{gi} and b_{gi} such that $F_g(0) = 0$.
- P_g^t is the active power generation of unit g at time t, in MW,
- θ_v^t is the voltage angle of node v in radians and at time t,
- C_g^0 is the no-load cost of unit g at time t, that is the cost of a unit that is active ($u_g^t = 1$) but that is not generating ($P_g^t = 0$). A classic example is a synchronous condenser, which can be synchronised at $P_g^{min} = 0$,
- R_g^t is the available Primary Frequency Response of unit g at time t, in MW. C_g^+ is the cost associated with the day ahead PFR offered.
- $\delta_g(P_g^t - P_g^{t-1}) := C_g^{\delta+} \max(P_g^t - P_g^{t-1}, 0) + C_{gt}^{\delta-} \max(P_g^{t-1} - P_g^t, 0)$ represents the ramp up and down reserve cost functions for each unit g in time t. Both are dispatch-dependent of P_g^t.

Physical constraints

$$u_g^t P_g^{\min} \leq P_g^t \tag{2}$$

$$P_g^t + R_g^t \leq P_g^{\max} u_g^t \tag{3}$$

$$0 \leq R_g^t \leq \min(R_g^{\max}, \Delta_g^{\max}), \tag{4}$$

$$\sum_{g \in \mathcal{G}_v} P_g^t - P_{Dv}^t - \sum_{\substack{w \in \mathcal{M} \\ v \neq w}} B_{vw}(\theta_v^t - \theta_w^t) = 0, \qquad \forall v \in \mathcal{M} \tag{5}$$

$$B_{vw}(\theta_v^t - \theta_w^t) \leq L_{vw}^{\max}, \qquad \forall\, v, w \in \mathcal{M} \tag{6}$$

$$\delta_g^{\min} \leq P_g^t - P_g^{t-1} \leq \delta_g^{\max}, \tag{7}$$

$$u_g^t - u_g^{t-1} \leq u_g^{\tau_g^1} \qquad \forall\, g \in \mathcal{G}; \qquad t \in \{2, \ldots, T-1\}; \qquad \tau_g^1 \in \{t+1, \ldots, \min\{t + \Lambda_g - 1, T\}\} \tag{8}$$

$$u_g^{t-1} - u_g^t \leq 1 - u_g^{\tau_g^0} \qquad \forall\, g \in \mathcal{G}; \qquad t \in \{2, \ldots, T-1\}; \qquad \tau_g^0 \in \{t+1, \ldots, \min\{t + \phi_g - 1, T\}\} \tag{9}$$

where we used the following constants:

- $P_g^{\min}$ is the lower limit of active power generation of unit g at time t, in MW (can be zero),
- $P_g^{\max}$ is the upper limit of active power generation of unit g at time t, in MW,
- $\mathcal{G}_v$ is the set of generators connected to node v,
- P_{Dv}^t is the power demand of node v at time t, in MW,
- B_{vw} is the susceptance of transmission line (v, w) in S,
- $L_{vw}^{\max}$ is the thermal limit of transmission line from bus v to w, in MW,
- $\mathcal{M}$ is the set of nodes, and $\mathcal{G}_v \subseteq \mathcal{G}$ is the set of generators connected to node $v \in \mathcal{M}$,
- $R_g^{\max}$ is the available offer of primary frequency response of unit g, in MW,
- $\Delta_g^{\max}$ is the physical capacity of primary frequency response of unit g, in MW,
- $\delta_g^{\max}$ upward physical limit of ramping capacity of unit g, in MW/h,
- $\delta_g^{\min}$ downward physical limit of ramping capacity of unit g, in MW/h,

- Λ_g is the minimum time the unit must be online after being connected to the system,
- ϕ_g is the minimum time the unit must be offline after being disconnected from the system,

The nonlinear functions S_g, F_g, and δ_g can be transformed into linear form with additional constraints and variables as follows. In its MILP linearised form, eq. (1) becomes:

$$\min_{\Phi'} \sum_{t\in\mathcal{T}}\sum_{g\in\mathcal{G}} \left(C_g^{S+}S_{gt}^{+} + C_g^{S-}S_{gt}^{-} + f_g^t + C_g^0 u_g^t + C_g^{+}R_g^t + C_g^{\delta+}\delta_{gt}^{+} + C_g^{\delta-}\delta_{gt}^{-}\right) \tag{10}$$

where $\Phi' := (S_{gt}^{+}, S_{gt}^{-}, P_g^t, f_g^t, R_g^t, u_g^t, \delta_{gt}^{+}, \delta_{gt}^{-}, \theta_v^t)_{g\in\mathcal{G}, t\in\mathcal{T}, v\in\mathcal{M}}$. We use the standard transformation to turn a maximum of linear functions into an auxiliary variable and a set of linear inequalities [31, pp. 150-151].

Auxiliary constraints

$$S_{gt}^{+} \geq u_g^t - u_g^{t-1}, \tag{11}$$
$$S_{gt}^{+} \geq 0, \tag{12}$$
$$S_{gt}^{-} \geq u_g^{t-1} - u_g^t, \tag{13}$$
$$S_{gt}^{-} \geq 0, \tag{14}$$
$$f_g^t \geq a_{gi}P_g^t + b_{gi}, \qquad \forall i \in \{1,\dots,n_g\} \tag{15}$$
$$\delta_{gt}^{+} \geq P_g^t - P_g^{t-1}, \tag{16}$$
$$\delta_{gt}^{+} \geq 0, \tag{17}$$
$$\delta_{gt}^{-} \geq P_g^{t-1} - P_g^t, \tag{18}$$
$$\delta_{gt}^{-} \geq 0, \tag{19}$$

where:

- S_{gt}^{+}, S_{gt}^{-} are the startup and shutdown auxiliary variables for unit g at time t, respectively,
- a_{gi}, b_{gi} denote the power-cost coefficients of generator g,
- f_g^t is the auxiliary cost variable of generator g.
- δ_{gt}^{+} is the ramp up auxiliary variable of unit g in time t, in MW,
- δ_{gt}^{-} is the ramp down auxiliary variable of unit g in time t, in MW.

2.2. Inclusion of frequency stability constraints

Next we analyse the frequency stability constraints to be included in the UC formulation. In order to ensure a minimum of inertia in the system that is capable to respond to a frequency excursion, is necessary to include this constraint in the UC problem. This new constraint must be linear as well. First is necessary to define where is this value present in the power system. We know that the so called swing equation dictates the dynamics of the frequency changes and power imbalances in the system. This equation is a first order ODE as shown in eq. (20):

$$P_a = P_m - P_e \tag{20}$$

where

- P_m is the mechanical power in MW,
- P_e is the electrical power in MW,
- P_a is the accelerating power in MW.

Since the combined inertia of the generator and the turbine is accelerated by this imbalance in power, and also causing a change of frequency, eq. (20) becomes:

$$\frac{2H}{f_0}\frac{d\Delta f(t)}{dt} + D\,P_D\,\Delta f(t) = P_m - P_e \tag{21}$$

where:

- H is the inertia in the system, in MW · s,
- f_0 is the system nominal frequency in Hz, which is 50 Hz in this study,
- P_m is the mechanical response from generators, in MW,
- P_e is the electrical imbalance, in our case unit tripped, in MW
- D is the damping element, in 1%/Hz,
- P_D is the total power demand in the system, in MW.

The damping D indicates the sensitivity of the load to the frequency problem, i.e., load that is susceptible to be disconnected from the grid due to large frequency excursions. This includes loads such as motors, which represent a heavily inductive element. Selecting a damping value of 1% from the total load is an approximation of the actual value of the nonlinear load that can be disconnected in the light of a generator or interconnector outage.

2.3. Rate of Change of Frequency constraint

For steady state purposes, we can define that the change in power is a result of a loss of generation in the system. Therefore, eq. (21) can be represented as in:

$$\Delta P_L^{max} = P_a = P_m - P_e \tag{22}$$

Following National Grid's grid code regulations, the maximum Rate of Change of Frequency $RoCoF_{max}$ acceptable in the system is set at 0.5 Hz/s. Notice that from now on, we have dropped the t superscript, considering that these calculations are performed for each time point in the planning horizon.

The available inertia in the system is calculated as in:

$$H = \sum_{g\in\mathcal{G}} H_g P_g^{max} u_g - \Delta P_L^{max} H_L^{max} + P_g^{wind} H_g^{wind} \tag{23}$$

where:

- H is the total inertia in the system after an outage in MW · s,
- H_g is the inertia per generator g, in MW · s,
- P_g^{max} is the rated power of unit g, in MW,
- ΔP_L^{max} is the maximum lost unit generation, in MW, known in advance in our work, and this is further elaborated in section 3,
- H_L^{max} is the maximum lost inertia of ΔP_L^{max}, in MW · s, known in advance in our work, and this is furter elaborated in section 3,
- P_g^{wind} is the power output of wind farm generator g,
- H_g^{wind} is the available synthetic inertia of wind farm generator g.

As a result of a unit outage in the power system, a mismatch between generation and demand arises. This leads to excursions of frequency in the system. In the very short term the response of the governors in the generators is negligible. The first value to alleviate this mismatch is the inertia. Therefore, the maximum RoCoF is proportional to the power lost and inversely proportional to the system inertia. The next step is to substitute eq. (22) and eq. (23) in eq. (21) This minimum level of inertia based on a maximum RoCoF requirement is obtained in:

$$H \geq \left| \frac{\Delta P_L^{max} f_0}{2RoCoF_{max}} \right| \tag{24}$$

This is now a linear constraint which can be added to the UC problem and the mixed integer linear programming formulation directly.

2.4. Frequency Nadir constraint inclusion

From eq. (21) now P_m can include two elements, such as the total enhanced frequency response in the system R_s^{tot} which is the response from storage units, and the total primary frequency response in the system R_g^{tot} which is the governor's response in the conventional generators. Both values are obtained for each time point of the UC optimisation. The storage units in this work are considered as the Battery Energy Storage systems (BESS), which quoting the IEEE standard, is defined as *"A system which is used to store electric energy by means of electrochemical materials, typically includes batteries, power conversion system, and battery management system"*. Consequently, taking into account the two responses, eq. (21) turns into:

$$\frac{2H}{f_0}\frac{d\Delta f(t)}{dt} + DP_D\Delta f(t) = R_S^{tot} + R_G^{tot} - \Delta P_L^{max} \tag{25}$$

where $\mathcal{S}$ is the set of available storage units to respond after a power imbalance, and $\mathcal{G}$ are the available conventional units. These two values happen in certain time point t each one according to:

$$R_S^{tot} := \begin{cases} \sum_{s\in\mathcal{S}} R_s t/T_s & \text{if } t \leq T_s \\ \sum_{s\in\mathcal{S}} R_s & \text{if } t > T_s \end{cases} \tag{26}$$

$$R_G^{tot} := \begin{cases} \sum_{g\in\mathcal{G}} R_g t/T_g & \text{if } t \leq T_g \\ \sum_{g\in\mathcal{G}} R_g & \text{if } t > T_g \end{cases} \tag{27}$$

where

- R_S^{tot} is the total response from storage units in MW, for each time point
- T_s is the delivery time from storage units in seconds s,
- R_G^{tot} is the total response from conventional units in MW, for each time point
- T_g is the delivery time from units in seconds s.

Assuming that t^* is the time when nadir happens, this time should range in the interval of $t \in [T_s, T_g)$ without actually reaching the governor time T_g. If the nadir occurs at time T_g this would have already activated the low frequency demand disconnection schemes, since the recovery of the frequency did not start after inertia had arrested the effect of the power imbalance. Hence for Frequency Nadir we have eq. (28):

$$\left|\Delta f_{nadir}\right| = \left|\Delta f(t = t^*)\right| \leq \Delta f_{max} \tag{28}$$

Now we identify the different regions of action from $R_s(t)$ and $R_g(t)$. Four sections have been depicted in fig. 1. The first to react is the $R_s(t)$ until it reaches its full response. This power changes with time, according to the ratio t/T_s, until it reaches its full output R_s at time T_s. Then a similar approach happens with the $R_g(t)$. Two sections can also be identified, but in this case we must remember that T_g is not fully reached. The rest of the frequency will be recovered by the secondary and tertiary frequency responses. At the nadir the system frequency reaches the lowest point after the largest generation or interconnector loss. At time t^*, the RoCof must be zero, since the frequency changing speed

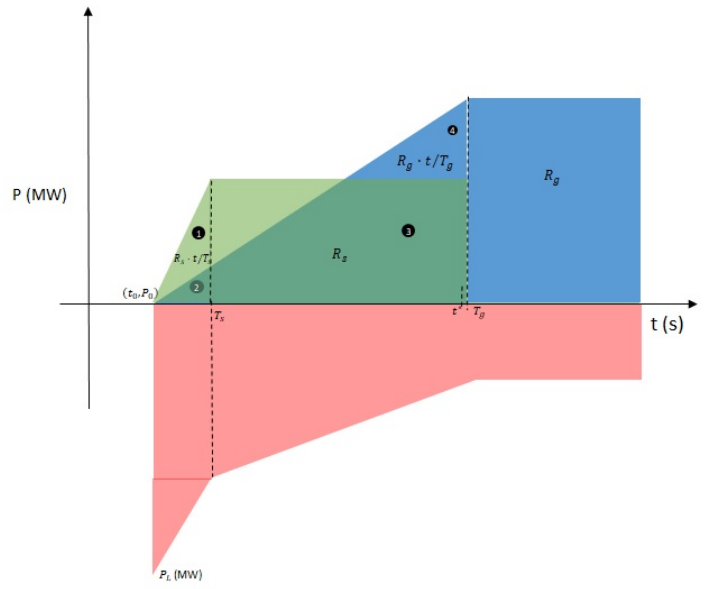

Figure 1: Power response vs. Power imbalance

stops. Also, in a conservative approach and for the sake of simplicity of the equation, we can assume no damping D effect is present. Thus, with these considerations in mind we can integrate eq. (25) and we have:

$$\Delta f(t^*) = \frac{f_0}{2H}\left[R_G^{tot}\frac{(t^*)^2}{2\,T_g} + R_S^{tot}(t^* - \frac{T_s}{2}) - \Delta P_L^{max} t^*\right] \tag{29}$$

Now, certain considerations must be done for eq. (25). Assuming the system frequency is at the nadir, now $\Delta f(t^*)$ should be zero and full power output from the storage units has been reached, so the time when the nadir occurs is:

$$t^* = \frac{T_g}{R_G^{tot}}(\Delta P_L^{max} - R_S^{tot}) \tag{30}$$

Substituting eq. (30) in eq. (29) we have:

$$\Delta f(t^*) = \frac{f_0}{2H}\left[-\frac{T_g}{2R_G^{tot}}(\Delta P_L^{max} - R_S^{tot})^2 - \frac{R_S^{tot}T_s}{2}\right] \tag{31}$$

Next, substituting eq. (31) in eq. (28) we have:

$$\left(\frac{H}{f_0} - \frac{R_S^{tot}T_s}{4\Delta f_{max}}\right)R_G^{tot} \geq \frac{T_g(\Delta P_L^{max} - R_S^{tot})^2}{4\Delta f_{max}} \tag{32}$$

And this is the case when we consider energy storage. Now we analyse the case with the governor response from conventional generators only. We can integrate eq. (25), and if we include the damping effect in eq. (32) then we have:

$$H\,R_G^{tot} - \frac{f_0\,T_g(\Delta P_L^{max})^2}{4\,\Delta f_{max}} + \frac{D\,P_D\,T_g\,\Delta P_L^{max}\,f_0}{4} \geq 0 \tag{33}$$

Equation (33) is a separable function where every term is constant but the product $H\,R_G^{tot}$. In appendix A we show the example of linearisation for a single variable, such as $(\Delta P_L^{max})^2$ assuming that the largest infeed is a variable in the

optimisation problem. The specific case of the product of two continuous variables is shown in appendix B, which is the case of our test system. The product $H R_G^{tot}$ is suitable to be represented as in the next change of variables:

$$H \alpha R_G^{tot} \beta = x_1^2 - x_2^2 \tag{34}$$

$$\frac{x_1 + x_2}{\alpha} = H \tag{35}$$

$$\frac{x_1 - x_2}{\beta} = R_G^{tot} \tag{36}$$

This is now a separable function that we linearise in the same fashion as the $(\Delta P_L^{max})^2$ value from the example of appendix A. The variables x_1 and x_2 are obtained in their linearised form as in eq. (B.1) and eq. (B.2), from the appendix B, respectively. The factors α and β help by scaling the difference between inertia H and the reserve R_G^{tot} bounds, assuming that they are in per unit values. This helps to improve the numerical stability of the solution. The boundaries of the new variables $H(x_1, x_2, \alpha)$ and $R_G^{tot}(x_1, x_2, \beta)$ for the UC optimisation are:

$$H_{min} \leq \frac{x_1 + x_2}{\alpha} \leq H_{max} \tag{37}$$

$$R_{Gmin} \leq \frac{x_1 - x_2}{\beta} \leq R_{Gmax} \tag{38}$$

Finally, substituting eq. (34) in eq. (33) we have:

$$x_1^2 - x_2^2 \geq f^* \tag{39}$$

where f^* in eq. (39) is:

$$f^* = f(f_0, T_g, \Delta P_L^{max}, \Delta f_{max}, \alpha, \beta)$$

Bearing in mind that f^* is in function of the values in eq. (33) and this is calculated for each time point t. Equation (24) changes to the following form substituting eq. (35) in it:

$$\frac{x_1 + x_2}{\alpha} \geq \left| \frac{\Delta P_L^{max} f_0}{2 RoCoF_{max}} \right| \tag{40}$$

Next, we analyse the constraint of the steady-state minimum frequency recovery.

2.5. Steady-state minimum frequency recovery

According to eq. (21), the third constraint depicts the behaviour of the frequency when the strategy aims to recover the frequency to a minimum acceptable value. This minimum acceptable recovery value of frequency is the difference between the nominal frequency and the aimed frequency in post-disturbance state, Δf_{ss}. For this constraint, it is correct to assume that the frequency excursion has been arrested, therefore the RoCoF it is zero. This third and last constraint solely depends on the amount of PFR available from the units, and it is also a linear constraint.

$$\frac{x_1 - x_2}{\beta} \geq \Delta P_L^{max} - D\, P_D\, \Delta f_{ss} \tag{41}$$

In the next section we show the study case with its respective results.

2.6. Literature comparison of Frequency Nadir handling

As mentioned in the introduction, recently published papers have approached Frequency Nadir linearisation in novel ways. To compare these works with our current paper, we show in table 1 the similarities and differences between these approaches. Our work follows the formulation of the frequency stability constraints of the works shown in the table, but we handle the Frequency Nadir non linearity in a different manner.

Table 1
Comparison of works on nadir linearisation

	Works on nadir linearisation		
concept	Badesa et al 2019[17]	Badesa et al 2020[18]	Ferrandon et al 2021
nadir linearisation technique	overestimating planes, binary expansion with big-M method	mixed integer second order cone program (MISOCP)	separable programming and SOS2 conditions
modelled problem	MILP	MISOCP	MILP
test system used	GB 2030 system	GB 2030 system	RTS updated version[24]
inclusion of synthetic inertia provision	✓	✓	✓
inclusion of storage response	✓	✓	✓*
scheduling time	Four months	one year	5 working days
load damping inclusion	✓	✓	✓
stochastic approach	✓	✓	✗

*Modelled, but not included in this work

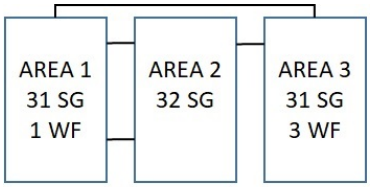

Figure 2: Three area RTS schematic diagram

3. Case Study

We work with the modified and updated version of the IEEE-RTS-96 power system [32, 24]. Physical capabilities and cost-related information of the power plants are included in updated version of the test system, which consider also the wind farms. In our work, we only consider the fuel costs of the power plants, so in the case of renewable energy generation it is set as zero. We do not consider fixed costs of the power plants for this UC problem, with the only exception of the start up and shut down costs. If the reader is interested in studies that include the fixed costs of renewable energy sources, some of this information can be found in [33]. UK grid code is applicable to this system, as is the case in [16]. We use the three-area version, including 95 synchronous generators and 4 wind farms located at different nodes in the system. The rotational inertia is provided by the synchronous generators and we have considered synthetic inertia by the wind farms. This system depicts how a power system is starting its transition to non-synchronous renewable energy sources, since the majority of the generators are conventional ones. The system is shown in an schematic diagram in fig. 2.

Using the IEEE-RTS-96 test system, we simulated a scheduling period of 5 days (120 hours) during the working week, whereas the costs, mean values of aggregated system inertia (H_{agg}), PFR provision, convergence times and total wind energy in the simulation are reported in table 3 and table 4. We worked with the base case, which has no frequency stability constraints, and four cases with frequency stability constraints but different levels of synthetic inertia provision. We selected the framework of the working-days week because in such scenario demands follows a more consistent pattern than during weekends. A long-term UC problem can deliver a scheduling of one year, as it is the case of [34], but in this study we wanted to observe the behaviour of a UC with frequency stability constraints for a week, more towards what the control room operators have to work with on a short-scale scheduling [35].

At the moment, we only consider the outage of the largest in-feed in this system, which is the nuclear power plant comprising for 400 MW, following an $N-1$ security criterion. The list of power plants of this test system is shown in

Table 2
Power plants available in the RTS-96 (updated [24] version)

Unit Group	figures acronym	Pmax per gen (MW)	Unit Type	Category	Fuel	number of power plants	inertia per gen (s)
U12	SG	12	Steam	Oil ST	Oil	7	2.8
U20	SG	20	CT	Oil CT	Oil	12	2.8
U50	Hydro	50	Hydro	Hydro	Hydro	19	3.5
U55	SG	55	CT	Gas CT	NG	27	2.8
U76	SG	76	Steam	Coal	Coal	7	3
U155	SG	155	Steam	Coal	Coal	7	3
U350	SG	350	Steam	Coal	Coal	2	5
U355	SG	355	CC	Gas CC	NG	10	7
U400	SG	400	Nuclear	Nuclear	Nuclear	1	5
Sync cond	n/a	0	Sync cond	Sync cond	Sync cond	3	0
Wind farm 1	Wind	713	Wind	Wind	Wind	1	6
Wind farm 2	Wind	847	Wind	Wind	Wind	1	6
Wind farm 3	Wind	122	Wind	Wind	Wind	1	6
Wind farm 4	Wind	799	Wind	Wind	Wind	1	6

Table 2. "CT" stands for "combustion turbine", whereas ""ST" means "steam turbine". "CC" is combined cycle power plant. In the second column of the table, the acronym "SG" stands for synchronous generators. Although the hydro power plants are synchronous generators as well, the distinction is made to observe the flexibility of intertemporal ramping and reserve that hydro sources add to the system. Although some of the the wind farms power outputs are larger than the nuclear power plant of the system, due to the transmission lines thermal limits these power outputs do not exceed the 400 MW. This is part of the UC optimisation results.

We use the next constants for the frequency stability constraints in the UC (they are following National Grid standards):

- nominal frequency (f_0) is 50 Hz,
- Delivery time (T_g) is 10 seconds,
- RoCoF is 0.5 Hz/s,
- Δf_{max} is 0.8 Hz,
- Δf_{ss} is 0.5 Hz.

Two scenarios with their respective sub-scenarios are considered in this work and the costs obtained are the total costs for the five days simulation. All the base cases in this paper were simulated with no synthetic inertia provision from wind power plants.

- High wind - low demand (HWLD),
  - Base case: no frequency stability constraints enforced, and no synthetic inertia provision from wind. The allocation of the PFR for this case is done under the criterion of minimum PFR of the [36], of at least 6% of the total load in the system. In the figures, this case is recognised as " HWLD" and "W/O FC",
  - Frequency stability constrained case, with synthetic inertia provision of $H_{wind} = 6\ s$ per wind farm. In the figures, this case is recognised as "HWLD" and "W/FC",
- High wind - high demand (HWHD),
  - Base case: no frequency stability constraints enforced, and no synthetic inertia provision from wind. The allocation of the PFR for this case is done under the criterion of minimum PFR of the [36], of at least 6% of the total load in the system. In the figures, this case is recognised as " HWHD" and "W/O FC",

Table 3
Results - HWLD

Case : High wind and low demand					
concept	base case	$H_{wind} = 0\,s$	$H_{wind} = 4\,s$	$H_{wind} = 5\,s$	$H_{wind} = 6\,s$
system cost	£4,955,261.77	£6,553,263.13	£6,551,028.37	£6,550,958.37	£6,545,450.76
reserves cost	£61,255.00	£224,980.00	£229,458.30	£228,648.43	£223,100.00
convergence time (s)	163	176.27	480.00	466.67	192.28
avg H_{agg} [min H_{agg},max H_{agg}] (s)	3.88 [3.51 4.64]	3.4 [3.12 4.31]	4.28 [4.26 4.36]	4.5 [4.37 4.547]	4.71 [4.38 4.83]
avg R_G^{tot} [min R_G^{tot}, maxR_G^{tot}] (MW)	355.98 [233.3 481.09]	1037.43 [1020.1 1055.84]	1035.24 [1016.75 1057.91]	1046.08 [1015.91 1217.71]	1034.55 [1015.07 1058.67]
wind energy (MWh)	177259.83	168090.46	167889.84	167889.77	167888.36

– Frequency stability constrained case, with synthetic inertia provision of $H_{wind} = 6\,s$ per wind farm. In the figures, this case is recognised as "HWHD" and "W/FC",

It is the interest of this work to understand how inertia and reserve will be allocated in the UC under frequency stability constraints with the extreme levels of demand, yielding a more robust approach toward security-constrained operations planning in systems with high wind injection. As a consequence, regarding the wind farms' high power injection levels for both levels of demand, we aimed to observe the impact of incorporating such frequency stability constraints in the light of high wind input. In the data from [24] we selected the working-days week that had the highest level of wind. The data is available for a whole year. For both cases of demand, we optimise for two sub-scenarios: one including synthetic inertia provision from wind and one without it. Synthetic inertia has been explained in the earlier part of this work. The simulation is run on a 64-bit Operating System, with an Intel(R) Core(TM) i5-8350U CPU at 1.70 GHz, with 8 GB of RAM.

3.1. High wind - low demand

The results for this simulation are shown in table 3. We performed a sensitivity analysis for different values of synthetic inertia provision from wind. Even for this case of low demand, where less units are connected to the system, the cost of increasing the units connected and the allocation of PFR increases compared to the unconstrained case.

3.1.1. Power profile

This is the power profile in the case without frequency constraints and including frequency constraints. They are shown in fig. 3a and fig. 3b, respectively. The hydro input adds a higher share of PFR in order to comply with the Frequency Nadir, which is the constraint that has a bigger weight in the simulation. It is important to highlight the RES penetration percentage, which can reach up to 50% in some time points.

3.1.2. RoCoF and inertia

RoCoF behaviour is purely limited by the inertia available in the system. We show the RoCoF and inertia level for both cases: with and without frequency constraint in the optimisation, in fig. 4a and fig. 4b, respectively.

Some observations from these graphs can be added. For the case of fig. 4a, and the yellow line, which is the case of frequency stability constraints, no inertia emulation provided by the 4 wind farms, the level of inertia is set by the conventional generators in the power system, which remain mostly constant throughout the simulation. Since conventional inertia for each generator is calculated as $P_g^{max} H_g u_g$, the value P_g^{max} is indeed constant, as well as H_g, hence the closeness to the RoCoF threshold and the little move of the RoCoF value.

On the other hand, when there is inertia emulation included in the simulation, such as $H_{wind} = 6s$ (blue line), the further the constraint is *pushed away* from the threshold. This can be observed using fig. 3a, between the hour 96 and

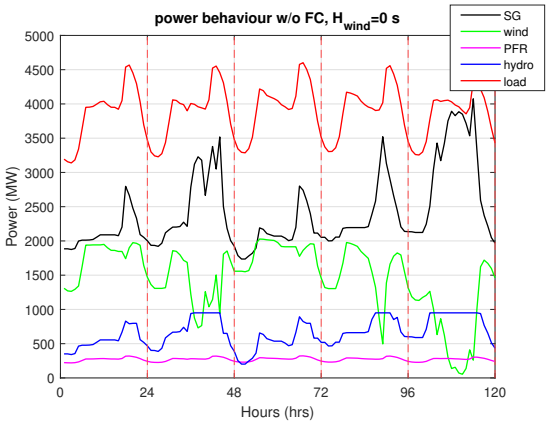

(a) Power profile without freq. constraints - HWLD

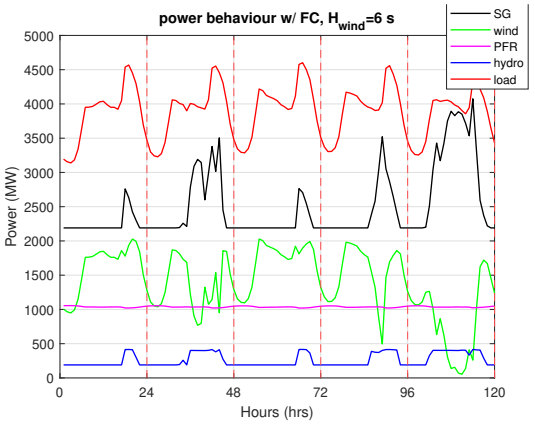

(b) Power profile with freq. constraints - HWLD

Figure 3: Power profiles - HWLD

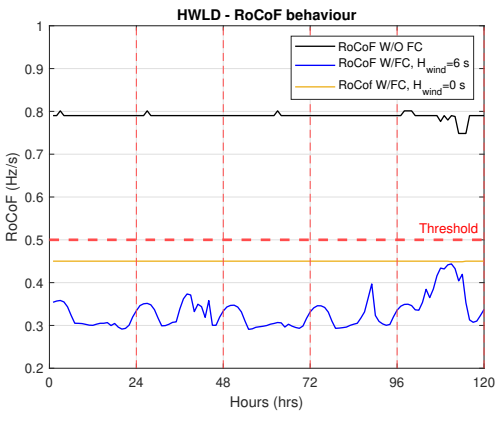

(a) RoCoF - HWLD

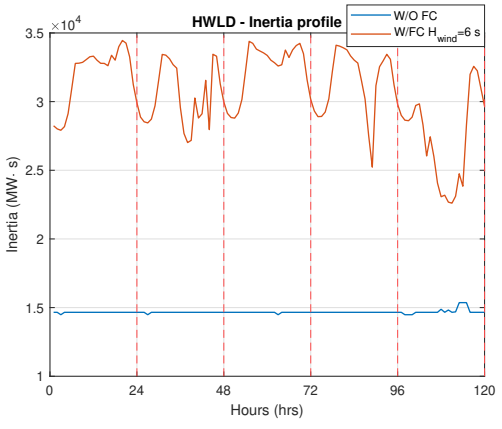

(b) Inertia - HWLD

Figure 4: RoCoF and inertia behaviour - HWLD

120. Under that time window, there is a dip in the active power of the wind farms, then the blue line in fig. 4a gets closer to the threshold. This inertia emulation injection to the grid depends on the available power output of the wind farms, as it can be seen in eq. (23), and there is no costs associated with this response for this work.

In our work, the frequency stability constraints are enforced from the beginning of the optimisation. This fully sets a minimum level of inertia to start with. Although the limit is to be no greater than 0.5 Hz/s, the actual value of the RoCoF is significantly lower than this value for the constrained case. We have to remember that this is a power system in the midst of its transition to RES, which is highlighted in the already fair amount of inertia for the case without frequency stability constraints. This is explained with the Frequency Nadir.

3.1.3. Frequency Nadir constraint, Δf_{nadir} and Δf_{max}

Now we observe the Frequency Nadir constraint. The nadir is lowest value that the nominal frequency in the power system can reach when a generation or interconnector outage occurs, shown in fig. 5 as Δf_{min}. For each time point of the simulation, we obtain the calculated value of Δf_{nadir}, from the resulting scheduling of the UC via eq. (33). Such value is shown in fig. 5, and its upper bound is shown in eq. (28), bounded by Δf_{max}. For example, a value of Δf_{nadir} of 0.25 Hz would imply, for a 50 Hz system, a Frequency Nadir of 49.75 Hz after a generation or interconnector outage.

The simulation's results on the Frequency Nadir constraint under the HWLD scenario are shown in fig. 6. The

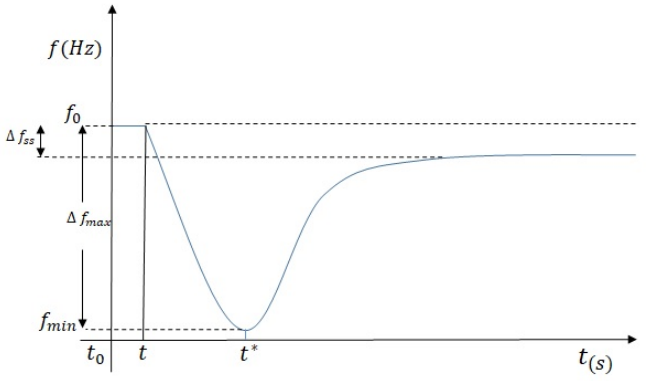

Figure 5: Frequency behaviour after a disturbance

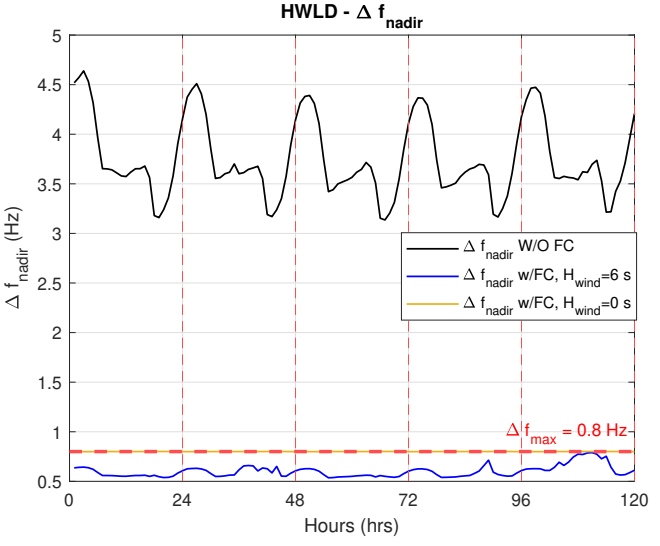

Figure 6: Frequency Nadir constraint behaviour - HWLD

product HR_G^{tot} controls the Frequency Nadir constraint. Via this product, the solution of the optimisation ensures that the frequency remains within bounds in the light of the largest in-feed from the day ahead perspective. This means that Δf_{nadir} is no greater than $\Delta f_{nadir} = 0.8\,\text{Hz}$ if such a contingency occurs. We can observe from the fig. 6 that in the case where there is a maximum of virtual inertia provision from the wind farms of the system, Δf_{nadir} is further away from the threshold of $\Delta f_{max} = 0.8\,\text{Hz}$ due to the fact that it has been assigned with zero cost in this problem. Again, due to the fluctuating power output value of P_g^{wind}, the total inertia provision in the system keeps changing, and combined with the PFR resource assigned, we obtain this calculated value of Δf_{nadir}. When there is no wind resource in the system, which is the case of the middle of the day of the last of the scheduling, there is no provision of virtual inertia and the Δf_{nadir} is controlled by the inertia from conventional generators and the PFR scheduled in the system. The inertia is obtained via eq. (23). The PFR available is provided only by the conventional generators. Furthermore, the time-dependant value of the load in eq. (33) also influences the Frequency Nadir constraint at each time point of the scheduling. Although this is not a transient stability analysis per se, and these are only the values of the constraints after the optimisation is performed, it is an approximation on how the system frequency behave. Compared to the case without frequency stability constraints, a higher frequency drop is present. Of course, before reaching these values of

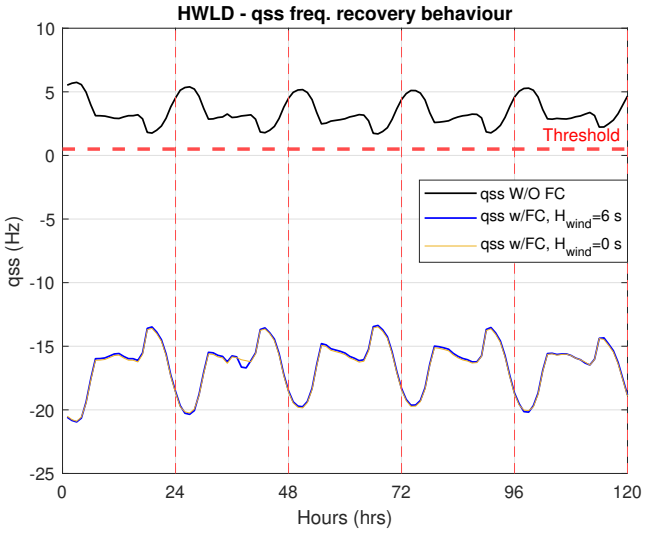

Figure 7: QSS behaviour - HWLD

Table 4
Results - HWHD

Case 2 : High wind and high demand					
concept	base case	$H_{wind} = 0\,s$	$H_{wind} = 4\,s$	$H_{wind} = 5\,s$	$H_{wind} = 6\,s$
system cost	£9,129,900.00	£9,752,400.00	£9,753,158.00	£9,715,261.00	£9,717,900.00
reserves cost	£88,661.00	£169,940.00	£170,348.00	£172,862.62	£172,070.00
convergence time (s)	45.07	273.11	254.47	334	351.6
mean H_{agg} [min ,max] (s)	3.88 [3.51 4.64]	5.03 [4.85 5.12]	5.03 [4.86 5.12]	5.05 [4.88 5.14]	5.02 [4.85 5.11]
mean R_G^{tot} [min, max] (MW)	355.98 [233.3 481.09]	701.12 [676.3 736.37]	701.69 [678.87 734.17]	706.02 [684.87 758.17]	707.243 [672.04 761.07]
wind energy (MWh)	160913.15	158479.40	158850.57	159146.45	167888.36

Frequency Nadir, the load shedding schemes come into play, which is a undesirable operational stance. Next we show the minimum value of frequency recovery.

3.1.4. QSS frequency recovery

This value solely depends on the amount of PFR available in the system. This will ensure the frequency is recovered to a maximum allowed deviation. This is shown in fig. 7. This constraint shows that there is no inertia involved, either in the form of conventional inertia or under inertia emulation provision from the wind farms. Thus, for both conditions in the system: maximum inertia emulation and no virtual inertia emulation, have no effect on the QSS frequency recovery. On the other hand, for both cases, the constraint remains under the established threshold.

In the next subsection we show the case for HWHD and its respective frequency stability constraints obtained.

3.2. High wind - high demand

This scenario shows the behaviour of the system with a high demand condition. This condition poses less severity on the $N-1$ contingency against an excursion of frequency, since in order to meet the demand it has to start from a different operational stance (more units connected from the beginning). The costs results are shown in table 4.

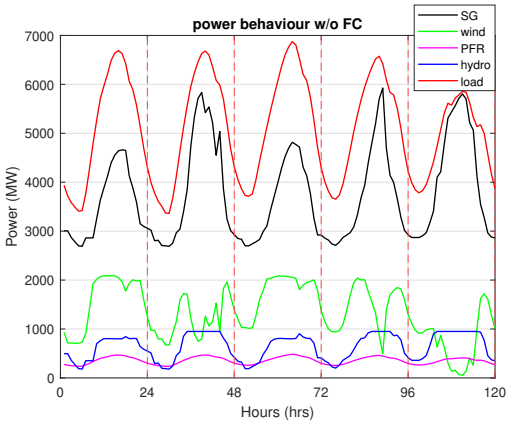

(a) Power profile without freq. constraints - HWHD

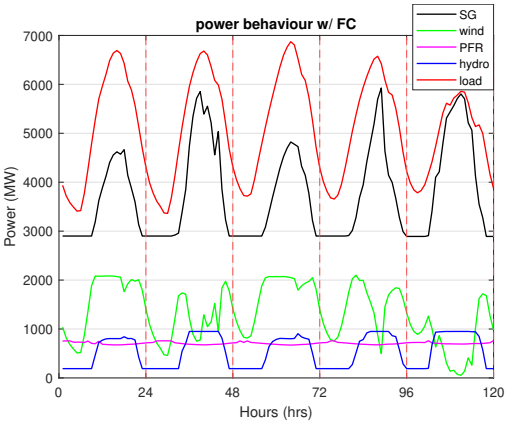

(b) Power profile with freq. constraints - HWHD

Figure 8: Power profiles - HWHD

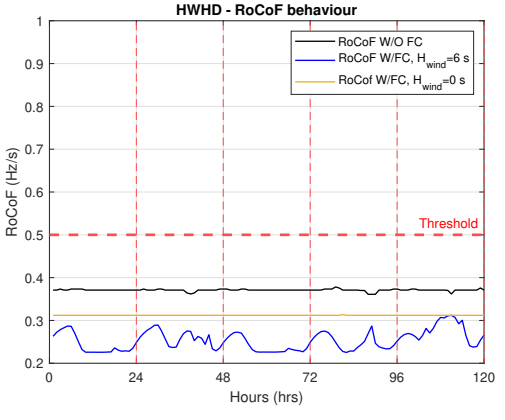

(a) RoCoF - HWHD

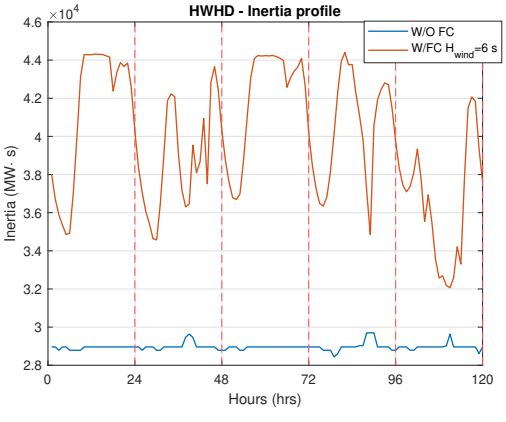

(b) Inertia - HWHD

Figure 9: RoCoF and inertia behaviour - HWHD

3.2.1. Power profile - HWHD

The high demand power profiles for the unconstrained and constrained cases are shown in fig. 8a and fig. 8b, respectively. When contrasting the previous case (low demand) with this current case (high demand), there is a lower value of PFR allocated for the high demand case. Although it might seem counter intuitive at first sight, we must acknowledge that the higher demand forces the solution to connect more units from the beginning of the optimisation, sharing the physical effort (inertia and PFR product) of arresting the Frequency Nadir in a different manner, compared to the low demand case. Furthermore, the hydro input plays a paramount role in the high demand case, responding to the inter-temporal ramping up and down constraints due to its faster responses.

3.2.2. RoCoF and Inertia - HWHD

The operational point the system starts under the high demand condition sets a different starting level of inertia in the system, compared to the low demand case. It is important to highlight that for both cases, synthetic inertia becomes a rather important player in the system that fluctuates following the wind behaviour pattern. With its inclusion on inertia provision, RoCoF value is kept in a lower value compared to the unconstrained and no synthetic inertia case. This is shown in fig. 9a and fig. 9b.

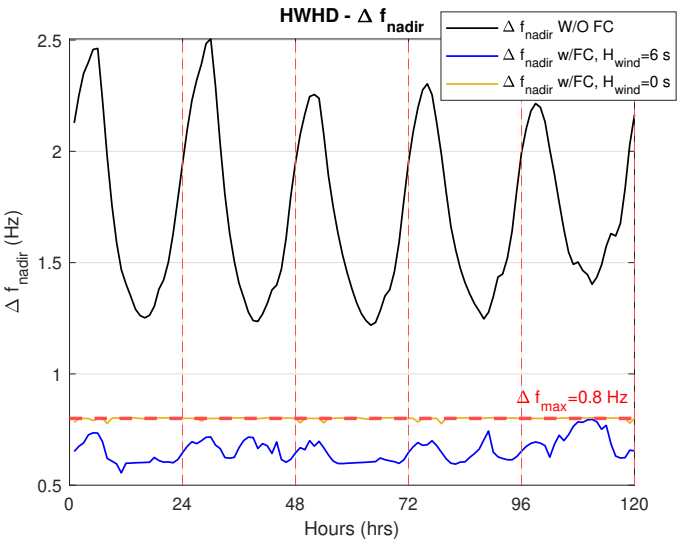

Figure 10: Frequency Nadir constraint behaviour - HWHD

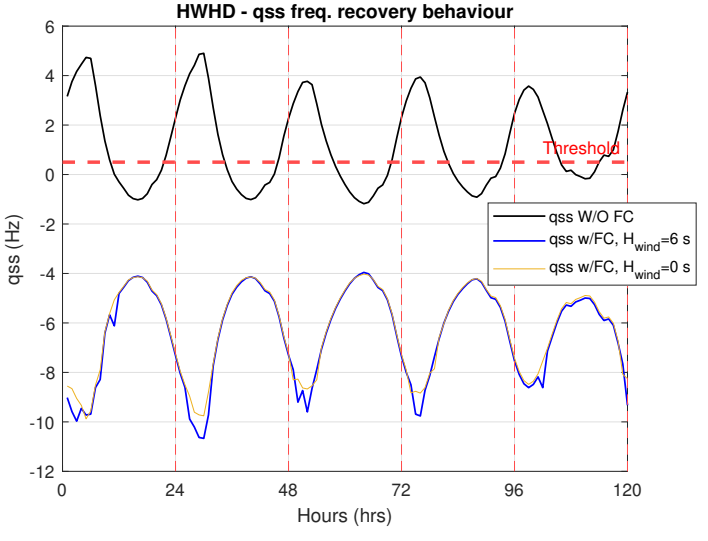

Figure 11: QSS behaviour - HWHD

3.2.3. Frequency Nadir - HWHD

The HDHW Frequency Nadir is shown in fig. 10. Again, without the share of synthetic inertia the system would be almost right over the constraint value (0.8 Hz). We see this behaviour at the times of low wind in the system, where the gap of the nadir and the constraint is reduced.

3.2.4. QSS frequency recovery - HWHD

In the HWHD case is shown that with lower share of PFR compared to the HWLD case, frequency can be recovered in minimum time previously set. This is shown in fig. 11.

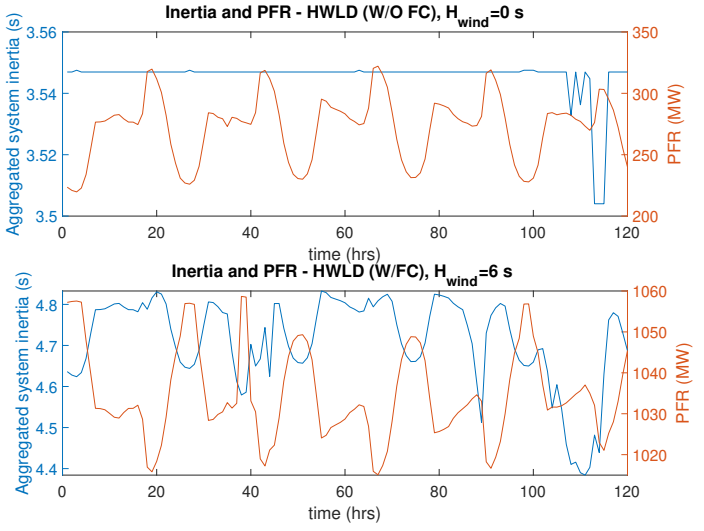

Figure 12: H and PFR interaction - HWLD

4. Discussion

4.1. Relevance of Frequency Nadir constraint

For both cases (HWLD and HWHD) the determinant constraint is the nadir. This is extremely important, because inertia only attenuates the speed of the frequency excursion, but it is the combination of inertia and PFR the one that arrests the frequency drop (nadir). The combination of both is bounded by the optimisation solution, so a lower value of PFR does not necesarily mean a higher frequency drop, since this low value of PFR should be covered by the available inertia in the system. This interaction between inertia and PFR is shown for HWLD and HWHD in fig. 12 and fig. 13, respectively.

4.2. Role of synthetic inertia in the UC with frequency stability constraints

While looking at the results obtained in table 3 and table 4 we notice the intrinsic value that the synthetic inertia has over the costs of running this test system. Four cases with frequency stability constraints and different values of synthetic inertia are run, ranging from 0 seconds, then from 3 to 6 seconds of inertia emulation from the wind farms. The highest value of inertia is taken from [16]. We do not intend to define a valuation method of the synthetic inertia for this test system. We do want to discuss how having an inertia emulation response affects the overall costs of the system. For this study, we did not assign any cost to the synthetic inertia. For the HWHD case, the solution indicates that the more synthetic inertia available, the higher input of wind is sought after in the optimisation, since both the variable costs and synthetic inertia from the wind have zero cost. This reduces the overall costs of the system, because it either reduces the use of units that do have non-zero variable costs, PFR costs, or both. For avoiding market distortions, it is necessary to do further studies on the synthetic inertia provision to define when this response becomes a necessity in the system, rather than just an "emulation" of natural inertia from conventional generators. Possibly, this scenario would be when the vast majority of the generation fleet comes from converter-based inputs, which is not the case of this transition-to-low-carbon system.

4.3. Role of PFR in the UC with frequency stability constraints

In this section, we will discuss how the Frequency Nadir and the QSS minimum frequency recovery constraints are influenced by the scheduled PFR in this test system. Recall that PFR together with the inertia available in the system controls the Frequency Nadir, i.e. how low the frequency can dip in a frequency excursion event. Figures 12 and 13 show the interaction between H and PFR. The Δf_{nadir} should be lower than the upper bound Δf_{max}, according to eq. (28). The PFR is bounded by eq. (7) and eq. (38). The total amount of PFR remains under the physical boundaries for each generator in our problem.

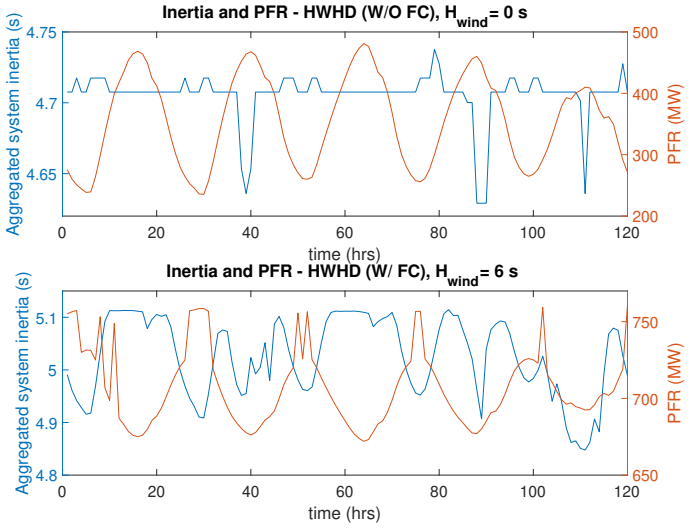

Figure 13: H and PFR interaction - HWHD

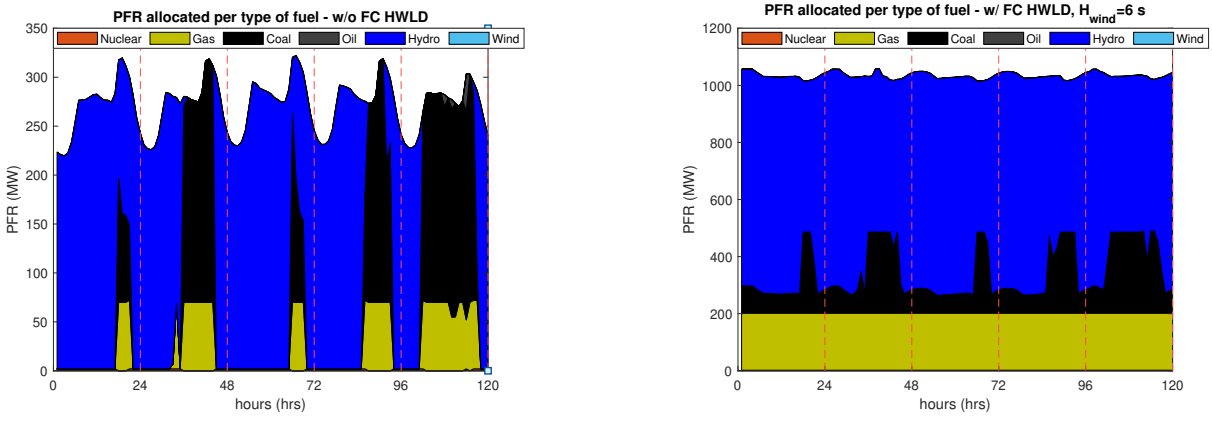

(a) Scheduled PFR without frequency constraints - HWLD

(b) Scheduled PFR with frequency constraints - HWLD

Figure 14: Scheduled PFR - HWLD

The Δf_{nadir} calculation from the Frequency Nadir constraint shown in figs. 6 and 10 is further away from the threshold because the virtual inertia coming from wind has not been assigned a cost in the system, and also because this virtual inertia provision is time-dependent through P_g^{max}. Moreover, the frequency constraints are enforced from the beginning of the problem. Therefore, the start up and shut down costs are concentrated at the beginning of the scheduling. Furthermore, the number of breaking points also have an influence on the amount of PFR allocated, as it will be further discussed in section 4.4. The more breaking points in the modelling, the tighter the difference between the maximum and minimum value of PFR allocated in the system throughout the simulation.

Secondly, we note that the QSS constraint is not binding for this specific problem and test system. Recall that PFR is in charge of handling the QSS constraint. However, due to the amount of PFR needed to control the Frequency Nadir, the QSS constraint is not binding, for both HWLD and HWHD scenarios. The scheduled PFR is allocated based on costs, amounts offered per generator, and ramping constraints. We show the distribution of PFR for the cases with and without frequency stability constraints of HWLD and HWHD scenarions in figs. 14a, 14b, 15a and 15b. The hydro resources are dominant due to its low costs and rapid ramping capabilities, compared to the rest of the generation fleet based on fossil fuels. We did not consider any PFR capabilities from wind resources. We can see that the PFR

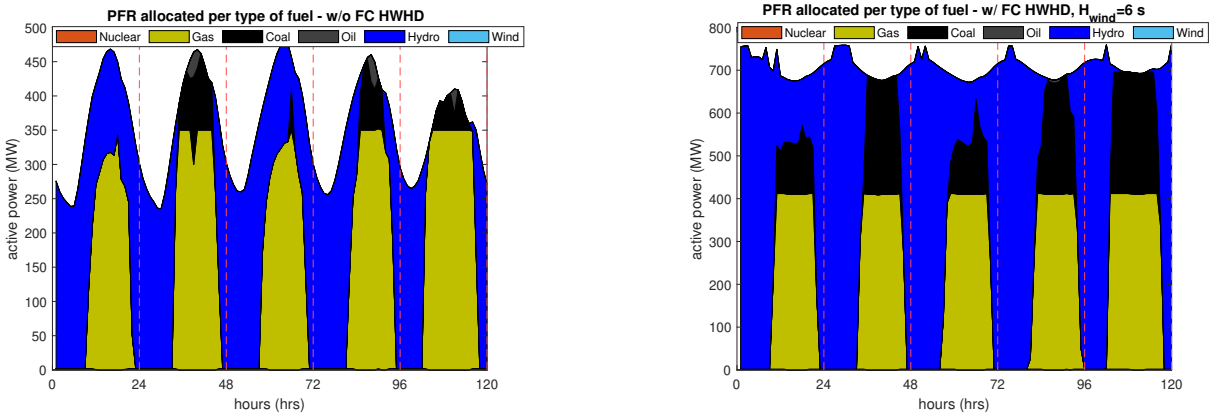

(a) Scheduled PFR without frequency constraints - HWHD

(b) Scheduled PFR with frequency constraints - HWHD

Figure 15: Scheduled PFR - HWHD

behaviour changes depending on the load scenario under analysis, showing a pattern of deeper dips in the middle of the day in the HWHD scenario. In fig. 15b we notice that in the last day of the scheduling, most of the PFR comes from fossil fuel sources. In fig. 8b, we observe that part of the peak demand is covered by hydro resources, and this coincides with dips in wind.

4.4. Linearisation breaking points

Now we observe the advantages and drawbacks of using less or more linearisation points in the separable programming problem. For the case of HWLD, we show the results from 5, 8, 10, 15, and 20 breaking points in table 5. Recalling that the problem is set with a duality gap of at least 2%, the case with 15 breaking points yields the smallest duality gap. Although choosing this approach would increase the convergence time by approximately 26 times the 10 breaking points case. In this scenario of HWLD, choosing a 5 breaking points approach would yield a better final duality gap, although the convergence time becomes an obstacle to use as a solution. We acknowledge that H_{agg} and R_G^{tot} remain very similar, regardless the selection of the number of breaking points. A cost-benefit analysis between the drawbacks and benefits of each thus lead us to choose to work with 10 breaking points for this scenario. In the case of the HWHD scenario, the solution with the lowest final duality gap uses the 10 breaking points scenario as well. For this scenario, the convergence time is quite similar between different breaking points, as well as the H_{agg} and R_G^{tot}. In this scenario, it is plausible to choose the 5 breaking points solution approach. although that would imply to have a higher duality gap. All in all, the number of breaking points for this work was calibrated upfront, depending mostly in two factors: final duality gap reached, and convergence time, and these factors are highly influenced by the scenario under analysis.

5. Conclusions and future work

In our work we have focused on looking for a new way of including the frequency constraints in the unit commitment optimisation process with the objective of minimising the system cost.The solution of the optimisation is within the physical boundaries of the system for purposes of ahead of real-time operations planning (in this case for five days). No time-domain simulation was performed, but the results can provide an starting point for a time-domain simulation. Via separable programming, this new approach approximates the non-linearity of the Frequency Nadir constraint to a linear form. The Frequency Nadir indicates the lowest value the frequency reaches after a generation or interconnector outage; whereas the Rate of Change of Frequency and Quasi-steady state frequency recovery constraints are both linear. The Frequency Nadir constraint involves the product of inertia and primary frequency response variables, then it becomes a non linear constraint and it cannot be added to the unit commitment formulation in its original form. Our approach consisted in tackling the non-linearity of the Frequency Nadir via separable programming. Depending on the power system to optimise, there is flexibility in the number of breaking points to use for the approximation of the linearisation. Tuning the number of breaking points and the scaling factors allows us to improve the convergence time

Table 5
Different number of linearisation breaking points - HWLD

Case : High wind and low demand, $H_{wind} = 6s$					
concept	5 bp	8 bp	10 bp	15 bp	20 bp
system cost	£6,509,749.81	£6,549,671.32	£6,545,450.76	£6,535,630.99	£6,625,835.55
reserves cost	£212,099.27	£223,556.53	£223,100.00	£221,721.38	£222,315.84
convergence time (s)	7501.74	62.4758124	192.28	5170.19	11481.985
duality gap	0.59%	1.71%	0.86%	0.18%	1.41%
mean H_{agg} [min ,max] (s)	4.711 [4.3768 4.8327]	4.711[4.3761 4.8326]	4.71 [4.38 4.83]	4.712 [4.380 4.832]	4.706 [4.376 4.828]
mean R_G^{tot} [min , max] (MW)	1003.94 [976.03 1221.25]	1033.80 [1014.659 1053.943]	1034.55 [1015.07 1058.67]	1030.55 [1011.96 1221.75]	1032.08 [1014.309 1052.078]
wind energy (MWh)	167905.84	168090.38	167888.36	167888.443	167484.714

Table 6
Different number of linearisation breaking points - HWHD

Case : High wind and high demand, $H_{wind} = 6s$					
concept	5 bp	8 bp	10 bp	15 bp	20 bp
system cost	£9,668,606.09	£9,757,420.05	£9,717,900.00	£9,784,849.62	£9,758,753.41
reserves cost	£172,161.55	£174,028.95	£172,070.00	£171,815.34	£171,448.83
convergence time (s)	164.88	428.094	351.60	356.81	340.40
duality gap	1.31%	1.77%	0.59%	2.00%	1.72%
mean H_{agg} [min,max] (s)	5.03 [4.85 5.12]	5.03 [4.86 5.12]	5.02 [4.85 5.11]	5.03 [4.85 5.12]	5.03 [4.85 5.12]
mean R_G^{tot} [min, max] (MW)	706.62 [681.08 766.08]	699.7 [678.2 888.58]	707.24 [672.04 761.07]	706.36 [679.61 735.87]	704.53 [679.61 736.38]
wind energy (MWh)	158867.42	159638.77	159709.75	159013.05	158847.54

of the problem. At every step, we made sure the system is covered against the loss of the largest in-feed under an $N-1$ security criterion. We included the transmission system constraints through, so we made sure that power flows remain below transmission line ratings from a DC load flow perspective. Our work has a practical application with power systems where the energy transition to a carbon neutral is at its early stage, and where we need to meet a minimum on-line commitment of units in the system for frequency stability and reliability reasons. This approach, along with the right electricity market framework, could incentivise new ancillary services such as inertia provision and different time windows of primary frequency response. This would help to avoid market distortions, by taking into account the inertia provision from renewable energy sources and the possible primary frequency response that they can deploy. We can expect to be necessary, for a low carbon grid, that the frequency stability is addressed not only by conventional generators, but from renewable energy sources too.

6. Acknowledgements

The authors greatly thank the reviewers and editor for their invaluable observations of this work which undoubtedly enriched its content.

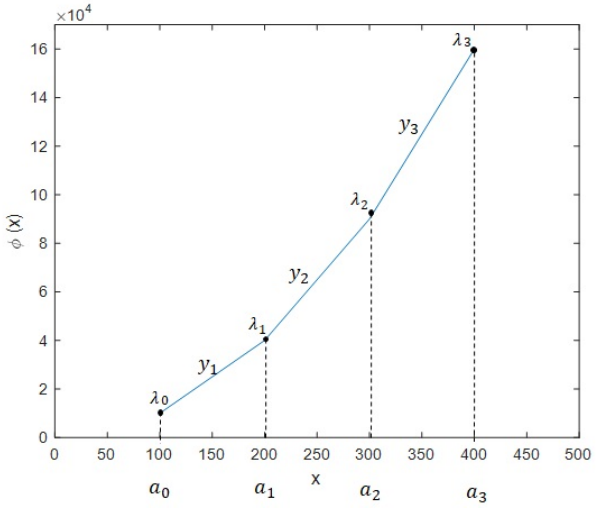

Figure 16: Discretisation of x value

A. Separable programming linearisation

In linear programming there is a way of including certain non-linearities, either in the objective function or the constraints. If the objective function or constraint to be minimised can be represented in the next form:

$$\phi(x_1, \dots, x_n) = \sum_{j=1}^{n} \phi_j(x_j) \tag{A.1}$$

is called a separable function. The j term stands for all the possible variables to be linearised in the objective function. For example, if the largest infeed $(\Delta P_L^{max})^2$ was a decision variable in the problem, we would need to linearise it to include it in the MILP, so the modelling would be:

$$x = \Delta P_L^{max} \tag{A.2}$$

$$\phi(x) = (\Delta P_L^{max})^2 \tag{A.3}$$

As a modelling strategy of approximating $\phi(x)$ as linear, we show the value of x as a piecewise linear function with some r affine segments, considering a range of outages of $[100, 400]$ MW for our system. This can be shown in fig. 16

First we perform a discretisation with lower l and upper u bounds of a_r values of the form $l \equiv a_0 < a_1 < \cdots < a_R \equiv u$. The more distance between each point, the better the approximation. Next we have to model the coordinates $(a_r, \phi(a_r))$ as a convex combination associated with the weights λ_r for each $r = 0, \dots, R$ and associate each transition between the a_r points with the binary variable y_r to reflect the selection of each affine segment in the interval $r = 1, \dots, R$. This formulation is shown as follows:

$$x = \sum_{r=0}^{R} a_r \lambda_r \quad \text{and} \quad \phi(x) \approx \sum_{r=0}^{R} \phi(a_r) \lambda_r \tag{A.4}$$

where:

$$\lambda_0 \le y_1, \quad \lambda_r \le y_r + y_{r+1} \text{ for all } r \in \{1, \dots, R-1\}, \quad \lambda_R \le y_R \tag{A.5}$$

$$\sum_{r=0}^{R} \lambda_r = 1, \quad \sum_{r=1}^{R} y_r = 1 \tag{A.6}$$

$$\lambda_r \ge 0, \quad y_r \in \{0, 1\}, \quad \text{for all } r \in \{0, 1, \dots, R\}; \tag{A.7}$$

The value of λ_r must meet the next condition:

Adjacency condition At most two λ_r weights are positive. If two weights are positive, then they are adjacent, i.e., of the form $\lambda_r + \lambda_{r+1}$. This is also known as a SOS2 *Special Ordered Set 2* condition. This whole approach will result in the approximation of the squared value of ΔP_L^{max}.

B. Frequency Nadir linearisation

Next, x_1 and x_2 are modelled using λ_{1r} and λ_{2r} operators to obtain the linearised form as in:

$$x_1 = \sum_{r=0}^{R} a_{1r}\lambda_{1r} \quad \text{and} \quad \phi_1(x_1) = x_1^2 \approx \sum_{r=0}^{R} a_{1r}^2\lambda_{1r} \tag{B.1}$$

$$x_2 = \sum_{r=0}^{R} a_{2r}\lambda_{2r} \quad \text{and} \quad \phi_2(x_2) = x_2^2 \approx \sum_{r=0}^{R} a_{2r}^2\lambda_{2r} \tag{B.2}$$

$$a_{1r} := \frac{r}{2R}(\alpha H_{max} + \beta R_{Gmax}), \quad \text{for} \quad r \in \{0, 1, \dots, R\} \tag{B.3}$$

$$a_{2r} := \frac{r}{2R}(\alpha H_{max} - \beta R_{Gmax}), \quad \text{for} \quad r \in \{0, 1, \dots, R\} \tag{B.4}$$

$$\lambda_{10} \le y_{11}, \quad \lambda_{1r} \le y_{1r} + y_{1,r+1}, \quad \text{for} \quad r = 1, \dots, R-1, \quad \lambda_{1R} \le y_{1R} \tag{B.5}$$

$$\lambda_{20} \le y_{21}, \quad \lambda_{2r} \le y_{2r} + y_{2,r+1}, \quad \text{for} \quad r = 1, \dots, R-1, \quad \lambda_{2R} \le y_{2R} \tag{B.6}$$

$$\sum_{r=0}^{R} \lambda_{1r} = 1, \quad \sum_{r=0}^{R} \lambda_{2r} = 1, \quad \sum_{r=1}^{R} y_{1r} = 1, \quad \sum_{r=1}^{R} y_{2r} = 1 \tag{B.7}$$

and

$$\lambda_{1r} \ge 0, \quad \lambda_{2r} \ge 0, \quad y_{1r} \in \{0, 1\}, \quad y_{2r} \in \{0, 1\}, \quad \text{for all } r \in \{0, 1, \dots, R\};$$

where:

- a_{1r} and a_{2r} are the breaking points in point r of the variables x_1 and x_2, respectively,
- λ_{1r} and λ_{2r} are the weights associated with each transition between breaking points a_{1r} and a_{2r} for breaking point r,
- y_{1r} and y_{2r} are the binary operators that select the affin segment of the linearisation,

and finally, the updated set of variables to optimise in the problem will be:

$$\Phi' := (S_{gt}^+, S_{gt}^-, P_g^t, f_g^t, R_g^t, u_g^t, \delta_{gt}^+, \delta_{gt}^-, \theta_v^t, \lambda_{1r}, \lambda_{2r}, y_{1r}, y_{2r})_{g\in\mathcal{G}, t\in\mathcal{T}, v\in\mathcal{M}, r\in R} \tag{B.8}$$

Table c.1
MOST settings

MOST settings
0. Set solver options
mpopt = mpoption(mpopt, 'most.dc_model', 1);
mpopt = mpoption(mpopt, 'gurobi.method', 2);
mpopt = mpoption(mpopt, 'gurobi.threads', 1);
mpopt = mpoption(mpopt, 'gurobi.opts.MIPGap', 0.02);
mpopt = mpoption(mpopt, 'gurobi.opts.MIPFocus', 2);
mpopt = mpoption(mpopt, 'gurobi.opts.Presolve', 2);
mpopt = mpoption(mpopt, 'gurobi.opts.PreSparsify', 1);
1. Load case
2. Set frequency stability constraints
3. Call modified MOST function
4. Get results

C. MOST general settings

A synthesised workflow of MOST is added for reference in table c.1. The solution was obtained for a 2% duality gap. For further references on the Gurobi solver settings, please see reference [37].

References

[1] The Crownstate, "Off shore wind electricity," 2017. [Online]. Available: https://www.thecrownestate.co.uk/energy-minerals-and-infrastructure/offshore-wind-energy/

[2] National Grid Electricity System Operator, *Future Energy Scenarios 2020*, National Grid ESO, July 2020. [Online]. Available: https://www.nationalgrideso.com/document/173821/download

[3] J. Cochran, M. Miller, O. Zinaman, M. Milligan, D. Arent, B. Palmintier, M. O´Malley, S. Mueller, E. Lannoye, A. Tuohy, B. Kujala, H. Holttinen, J. K. M. Sommer, and S. Soonee, "Flexibility in 21st Century Power Systems," *21st Century Power*, May 2014.

[4] National Grid Electricity System Operator, *National Grid Operability Strategy Report 2020*, National Grid ESO, November 2020. [Online]. Available: https://www.nationalgrideso.com/document/159726/download

[5] Jan Machowski and Janusz W. Bialek and James R. Bumby, *Power System Dynamics, Stability and Control*. John Wiley and Sons, 2008.

[6] P. Tielens and D. Van Hertem, "The relevance of inertia in power systems," *Renewable and Sustainable Energy Reviews*, vol. 55, pp. 999–1009, 2016. [Online]. Available: http://dx.doi.org/10.1016/j.rser.2015.11.016

[7] National Grid Electricity System Operator, *System Operability Framework 2019 - Past Frequency Events*, National Grid ESO, November 2019. [Online]. Available: \protect\protect\unhbox\voidb@x\hbox{https://www.nationalgrideso.com/document/156761/download}

[8] ——, *System Operability Framework 2019 - Operating a Low Inertia System*, National Grid ESO, February 2020. [Online]. Available: https://www.nationalgrideso.com/document/164586/download

[9] Office of Gas and Electricity Markets, *9 August 2019 power outage report*, Ofgem, January 2020. [Online]. Available: https://www.ofgem.gov.uk/system/files/docs/2020/01/9_august_2019_power_outage_report.pdf

[10] National Grid Electricity System Operator, *Mandatory response services*, National Grid ESO, July 2020. [Online]. Available: https://www.nationalgrideso.com/balancing-services/frequency-response-services/mandatory-response-services

[11] European Network of Transmission System Operator, *System Operator Guideline (SOGL)*, ENTSO-E, August 2017. [Online]. Available: https://www.entsoe.eu/network_codes/sys-ops/

[12] A. J. Wood, B. F. Wollenberg, and G. B. Sheble, *Power generation, operation, and control, 3rd Edition*. Wiley, 2014.

[13] Z. Chu, U. Markovic, G. Hug, and F. Teng, "Towards optimal system scheduling with synthetic inertia provision from wind turbines," *IEEE Transactions on Power Systems*, vol. 35, no. 5, pp. 4056–4066, 2020.

[14] J. Restrepo and F. Galiana, "Unit commitment with primary frequency regulation constraints," in *2006 IEEE Power Engineering Society General Meeting*, June 2006, pp. 1 pp.–.

[15] F. Teng, V. Trovato, and G. Strbac, "Stochastic scheduling with inertia-dependent fast frequency response requirements," in *2016 IEEE Power and Energy Society General Meeting (PESGM)*, July 2016, pp. 1–1.

[16] M. Paturet, U. Markovic, S. Delikaraoglou, E. Vrettos, P. Aristidou, and G. Hug, "Stochastic unit commitment in low-inertia grids," *IEEE Transactions on Power Systems*, pp. 1–1, 2020.

[17] L. Badesa, F. Teng, and G. Strbac, "Simultaneous scheduling of multiple frequency services in stochastic unit commitment," *IEEE Transactions on Power Systems*, vol. 34, no. 5, pp. 3858–3868, 2019.

[18] ——, "Optimal portfolio of distinct frequency response services in low-inertia systems," *IEEE Transactions on Power Systems*, vol. 35, no. 6, pp. 4459–4469, 2020.

[19] M. Malekpour, M. Zare, R. Azizipanah-Abarghooee, and V. Terzija, "Stochastic frequency constrained unit commitment incorporating virtual inertial response from variable speed wind turbines," *IET Generation, Transmission & Distribution*, vol. 14, no. 22, pp. 5193–5201, 2020.

[20] Z. Zhang, E. Du, F. Teng, N. Zhang, and C. Kang, "Modeling frequency dynamics in unit commitment with a high share of renewable energy," *IEEE Transactions on Power Systems*, vol. 35, no. 6, pp. 4383–4395, 2020.

[21] Y. Yin, T. Liu, L. Wu, C. He, and Y. Liu, "Frequency-constrained multi-source power system scheduling against n-1 contingency and renewable uncertainty," *Energy*, vol. 216, p. 119296, 2021.

[22] National Grid, "THE GRID CODE," 2020. [Online]. Available: https://www.nationalgrideso.com/industry-information/codes/grid-code

[23] F. Gonzalez-Longatt, "Impact of synthetic inertia from wind power on the protection/control schemes of future power systems: Simulation study," in *11th IET International Conference on Developments in Power Systems Protection (DPSP 2012)*, 2012, pp. 1–6.

[24] GRID Modernization Laboratory Consortium - US Department of Energy, "Updated ieee reliability test system," *GMLC*, 2017.

[25] C. E. Murillo-Sánchez, R. D. Zimmerman, C. L. Anderson, and R. J. Thomas, "Secure planning and operations of systems with stochastic sources, energy storage, and active demand," *IEEE Transactions on Smart Grid*, vol. 4, no. 4, pp. 2220–2229, Dec 2013.

[26] R. D. Zimmerman, C. E. Murillo-Sanchez, and R. J. Thomas, "Matpower: Steady-state operations, planning, and analysis tools for power systems research and education," *IEEE Transactions on Power Systems*, vol. 26, no. 1, pp. 12–19, Feb 2011.

[27] Yuping Huang and Panos M. Pardalos and Qipeng P. Zheng, *Electrical Power Unit Commitment - Deterministic and Two-Stage Stochastic Programming Models and Algorithms*. Springer, 2014.

[28] Igor Griva and Stephen G. Nash and Ariela Sofer, *Linear and nonlinear optimisation*. SIAM, 2009.

[29] David G. Luenberger and Yinyu Ye, *Linear and non-linear programming*. Springer, 2008.

[30] D. A. Tejada-Arango, S. Wogrin, P. Sánchez-Martın, and A. Ramos, "Unit commitment with acopf constraints: Practical experience with solution techniques," in *2019 IEEE Milan PowerTech*, 2019, pp. 1–6.

[31] S. Boyd and L. Vandenberghe, *Convex Optimization*. Cambridge University Press, 2009. [Online]. Available: https://web.stanford.edu/~boyd/cvxbook/bv_cvxbook.pdf

[32] C. Grigg, P. Wong, P. Albrecht, R. Allan, M. Bhavaraju, R. Billinton, Q. Chen, C. Fong, S. Haddad, S. Kuruganty, W. Li, R. Mukerji, D. Patton, N. Rau, D. Reppen, A. Schneider, M. Shahidehpour, and C. Singh, "The IEEE Reliability Test System-1996. A report prepared by the Reliability Test System Task Force of the Application of Probability Methods Subcommittee," *IEEE Transactions on Power Systems*, vol. 14, no. 3, pp. 1010–1020, Aug 1999.

[33] M. Hildmann, A. Ulbig, and G. Andersson, "Empirical analysis of the merit-order effect and the missing money problem in power markets with high res shares," *IEEE Transactions on Power Systems*, vol. 30, no. 3, pp. 1560–1570, 2015.

[34] F. Teng, V. Trovato, and G. Strbac, "Stochastic scheduling with inertia-dependent fast frequency response requirements," *IEEE Transactions on Power Systems*, vol. 31, no. 2, pp. 1557–1566, 2016.

[35] E. Vaahedi, *Power System Operation Optimization*. John Wiley & Sons, Ltd, 2014, ch. 8, pp. 119–150. [Online]. Available: https://onlinelibrary.wiley.com/doi/abs/10.1002/9781118915110.ch8

[36] Secretaría de Energia, *Código de Red*, Gobierno de México, 2016. [Online]. Available: https://www.cenace.gob.mx

[37] Gurobi Optimization, *Gurobi solver*, Gurobi, June 2021. [Online]. Available: https://www.gurobi.com/documentation/9.1/refman/parameters.html